Improved UWB TDoA-based Positioning using a Single Hotspot for Industrial IoT Applications

M. Martalò *Senior Member, IEEE*, S. Perri, G. Verdano, F. De Mola, F. Monica, and G. Ferrari *Senior Member, IEEE*

Abstract—The goal of this paper is to investigate Ultra Wide-Band (UWB) localization with Time Difference of Arrival (TDoA) processing at the anchors. We consider scenarios where the anchors are placed very close to each other and the target to be localized is around the group of anchors. All target-anchor communications are assumed to be in Line-Of-Sight (LOS). Since our analysis shows that symmetries in anchors' placement, with respect to the target position, degrade the positioning accuracy of standard algorithms, we propose to use a Subset Selection (SS) strategy, where position estimates obtained with properly selected subsets of asymmetric anchors are fused together to get the final localization output. Our results show improved localization accuracy with respect to the use of all anchors, especially in estimating the angle of arrival. Finally, we analyze the impact of an inaccurate time synchronization among the anchors, deriving guidelines for hardware implementation.

Index Terms—Smart Industry, Localization, Ultra WideBand (UWB), Time Difference of Arrival (TDoA), Subset Selection, Data Fusion, Synchronization.

I. INTRODUCTION

A key aspect in modern communication networks is user and object positioning to enable enhanced location-based applications [1]. The increasing interest towards the Internet of Things (IoT) and related relevant applications, such as smart buildings and industries, is pushing in this direction [2]–[6]. IoT-based solutions can be beneficial for industrial applications, leading to Industrial IoT (IIoT) and, more generally, enabling the Industry 4.0 paradigm. In fact, knowing the positions of users and objects inside a smart factory is a key enabling technology for factory automation. In this scenario, a multitude of low-energy low-cost devices and controllers cooperate to manage relevant factory processes, together various available Information and Communication Technologies (ICT) [7].

In particular, knowledge of users' and devices' positions may improve the safety in scenarios where people and autonomous systems coexist [8]. Besides the safety application considered in our work, localization can applied to different industrial contexts in combination with various technologies. In [9], a mitigation scheme for the impairments caused by

M. Martalò is with the Department of Electrical and Electronic Engineering, University of Cagliari, Italy, & the Research Unit of Cagliari, Consorzio Nazionale Interuniversitario per le Telecomunicazioni (CNIT), Italy, e-mail: marco.martalo@unica.it. He was with with the University of Parma, Italy, when this work was carried out. S. Perri, G. Verdano, F. De Mola, and F. Monica are with Elettric80 S.p.A., Viano (RE), Italy, e-mail: {perri.s,verdano.g,demola.f,monica.f}@elettric80.it.G. Ferrari is with the IoT Lab, Department of Engineering and Architecture, University of Parma, Italy, e-mail: gianluigi.ferrari@unipr.it.

typical industrial environments is proposed for a localization system based on Ultra Wideband (UWB) and Time Difference of Arrival (TDoA) technologies in commercial devices. In [10], modelling and simulation is proposed for a Received Signal Strength Indicator (RSSI)-based positioning system aimed at localizing Automatic Guided Vehicles (AGVs) in smart factory environments. In [11], localization is performed by relying on Radio Frequency IDentification (RFID) tags whose positions are estimated from the signal RSSI and phase.

Radio-based positioning accuracy may not be high in an indoor environment, because of signal propagation limitations (e.g., obstructions, multipath, and interferences) [12]. More generally, positioning can leverage existing radio network infrastructures, such as Bluetooth, WiFi, cellular (4G/5G) [13]. UWB technology is attractive, because of the high time resolution and, consequently, accurate target positioning in many scenarios [14], [15].

In radio-based positioning, the target position is obtained by estimating the distances between the target itself and reference nodes, referred to as *anchors*. Such distance estimation is performed on the basis of given signal characteristics, e.g., RSSI, Angle of Arrival (AoA), Time of Flight (ToF), TDoA [16]. In particular, in TDoA-based techniques the target transmits a beacon signal and the positioning system computes the difference between the propagation times at pairs of anchors, under the assumption of sufficiently accurate synchronization. Unlike methods based on the received signal strength, TDoA-based localization is more accurate and robust against environmental changes [17]. TDoA schemes with UWB communications have been exploited in various scenarios: see, for example, [18]–[21] and references therein.

Standard literature solutions consider "classical" scenarios, where the target lies inside the area to be monitored and the anchors are along the perimeter of the area itself. In this work, we consider a "non-classical" scenario in which the anchors are concentrated on a single "hotspot" with limited dimensions, whereas the target can move around it. This scenario is relevant for various applications in which anchors' placement along the perimeter of the area of interest may be costly or cannot be carried out. A relevant application scenario is in smart warehouses, where human operators and AGVs coexist. In this case, the anchors may be placed on the AGV to localize human operators around it. Even if the relative position between anchors and target is not relevant from a theoretical point of view, e.g., to determine the limiting performance in terms of Cramer-Rao Lower Bound (CRLB) [22], it influences the performance of a localization algorithm. In

fact, the presence of symmetries in the anchors' placement, with respect to the target position, can significantly degrade the localization accuracy [23], especially if the anchors are concentrated on a single hotspot.

We consider a scenario where multiple anchors are concentrated in a single hotspot and investigate the performance of TDoA-based UWB localization. This scenario has partial similarity with that in [24] (referred to as Large Equal Radius, LER), in which (i) the anchors are (almost) equidistant from a proper reference point and (ii) the distances from such a point are much longer than those from the anchors to the object to be located. However, even if in our scenario the anchors may be considered equally distant from the center of gravity of the hotspot, this distance is typically (much) shorter than each target-anchor distance. The main contributions of our paper can be summarized as follows: (i) an extensive performance analysis of various localization algorithms and schemes is carried out; (ii) a method, based on the idea of Subset Selection (SS), to avoid geometric symmetries of the anchors' relative positions, with respect to the target, is considered; and (iii) the impact of a synchronization error between anchors is investigated to derive hardware design guidelines. The key idea of the SS approach is to use a standard localization algorithm, but performing localization only considering a few properly selected anchors. In particular, various position estimates, obtained from different subsets of anchors, are considered. The best subset can be selected or the various estimates can be fused together to improve the overall localization accuracy. We refer to the latter approach as SS with Data Fusion (SSwDF). A state of the art TDoA 3D geometric algorithm is applied jointly with the considered SS strategy: our results show accurate estimation of the target angle of arrival with respect to the hotspot with a small estimation dispersion (i.e., error variance). The considered scheme is robust, given that the target position estimation error has an average relative error (with respect to the distance) smaller than 10% for a distance between target and hotspot up to 10 m. A significant performance improvement, in terms of localization accuracy, is achieved by using the considered SSwDF strategy, as shown by direct comparison with the corresponding theoretical CRLB.

The structure of this paper is the following. Section II is dedicated to the system model. In Section III, the considered SS strategy for improved localization is described. In Section IV, numerical results are presented. In Section V, the impact, on the positioning accuracy, of a synchronization error between the anchors is analyzed. Finally, in Section VI concluding remarks are given. In the remainder of this paper, the following notation will be used: boldface **lowercase** and **UPPERCASE** letters denote vectors and matrices, respectively; $\tilde{x}$ and $\hat{x}$ will denote the measurement and an estimate of the true value x, respectively.

II. SYSTEM MODEL

In Fig. 1, we show an illustrative representation of the considered scenario. The hotspot includes N anchors, whose
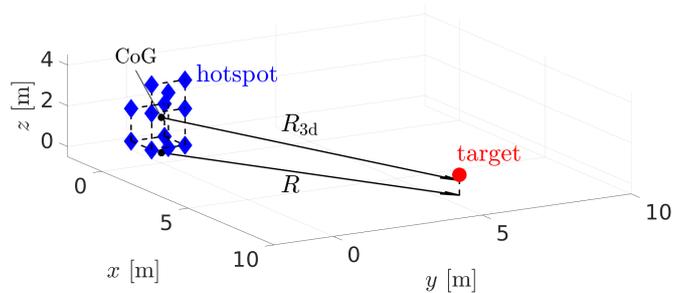

Fig. 1. System model: a target, equipped with UWB transceiver (red circle), is placed at distance (on the $x - y$ plane) R from an hotspot, equipped with N anchors (blue diamonds).

Cartesian coordinates are given by the following three-dimensional vectors:

$$\boldsymbol{a}_i = [a_x^{(i)}, a_y^{(i)}, a_z^{(i)}]^T \qquad i = 1, \dots, N$$

where T denotes the transpose operator. The target, placed around the hotspot, has coordinates given by the column vector $\boldsymbol{s} = [s_x, s_y, s_z]^T$. The estimated target position is instead denoted as $\hat{\boldsymbol{s}} = [\hat{s}_x, \hat{s}_y, \hat{s}_z]^T$. The distance r_i between the target and the i-th anchor can be expressed as follows:

$$r_i = ||\boldsymbol{s} - \boldsymbol{a}_i|| = c\tau_i \tag{1}$$

where $||\cdot||$ is the Euclidean norm, $c \simeq 3 \cdot 10^8$ m/s is the speed of light, and τ_i is the ToF between the target and the i-th anchor. The three-dimensional distance between the target and the hotspot (as group of anchors) is denoted as $R_{3d} \triangleq ||\boldsymbol{s} - \bar{\boldsymbol{a}}||$, where $\bar{\boldsymbol{a}}$ is the Center of Gravity (CoG) of the anchors:

$$\bar{\boldsymbol{a}} \triangleq \frac{1}{N} \sum_{i=1}^{N} \boldsymbol{a}_i.$$

Finally, we denote as R the two-dimensional distance between the projections of $\bar{\boldsymbol{a}}$ and $\boldsymbol{s}$ on the $x - y$ plane.

A. TDoA Measurements

As anticipated in Section I, TDoA algorithms do not rely on the absolute ToFs measured at the anchors after the reception of a target beacon, but on the relative differences between them.[1] Let us assume that $\boldsymbol{a}_j$ ($j \in \{1, 2, \dots, N\}$) is the first anchor receiving the beacon transmitted by the target. The TDoA between the i-th anchor and the reference one, denoted as $\Delta\tau_i$ ($i \neq j$), can be computed as the difference between the ToFs measured at the two anchors, i.e.,

$$\Delta\tau_i = \tau_i - \tau' \qquad i \in \{1, \dots, N\}/j \tag{2}$$

where τ' is the ToF at the reference anchor $\boldsymbol{a}_j$. Note that, by definition, $\Delta\tau_i > 0$. In practice, however, only measured TDoAs, rather than the true TDoAs, are available. These measured TDoAs are denoted as

$$\widetilde{\Delta\tau}_i = \tilde{\tau}_i - \tilde{\tau}' = \frac{\tilde{r}_i - \tilde{r}'}{c} \quad i \in \{1, \dots, N\}/j \,.$$

[1]Note that the number of anchors receiving the transmitted beacon may be smaller than N, e.g., due to environmental interference and obstacles. Without losing the generality of our approach, we assume that all anchors receive the beacon and can collaborate to target localization.

It is worth noting that the accuracy of (2) may be affected by limited clock synchronization between the anchors, i.e., the ToFs τ_i and τ' need to refer the same time axis [25]. In the following, we first assume that the anchors are perfectly synchronized with each other. In Section V, we then discuss on the impact of imperfect time synchronization among anchors, in order to derive hardware design guidelines.

B. UWB Communication Channel Model

The statistical characterization of the error noise in the measured distance $\tilde{r}_i$ ($i \in \{1, \ldots, N\}$) depends on UWB signalling and channel status. All the target-anchor communication links are assumed to be in Line-Of-Sight (LOS). In this paper, we consider the simple, yet accurate, statistical error model proposed in [26]. In particular, the noisy ToF measurement in the UWB LOS link between the target and the i-th anchor can be expressed as

$$\tilde{\tau}_i = \tau_i + \delta_i$$

where $\delta_i \sim \mathcal{N}(\mu_i, \sigma_i^2)$. Resorting to experiments with point-to-point two-way ranging, μ_i and σ_i^2 are shown to be approximately linear functions of r_i, i.e., [26]

$$\mu_i(r_i) \simeq q_1\tau_i + q_2/c = q_1\frac{r_i}{c} + \frac{q_2}{c} \qquad (3)$$

$$\sigma_i(r_i) \simeq \beta_1\tau_i + \beta_2/c = \beta_1\frac{r_i}{c} + \frac{\beta_2}{c}. \qquad (4)$$

Expressions (3) and (4) are intuitive, since the larger the nodes' distance, the higher the expected measurement noise. The parameters $\{q_1, q_2, \beta_1, \beta_2\}$ in (3)-(4) can be obtained using a standard Least Square (LS) estimation on experimentally acquired data.

In particular, we consider an experimental setup with a single link between decaWave DW1000 UWB nodes [27]. Applying the LS method described in [26] to approximately 10^3 transmissions, one obtains $q_1 = 0.0042$, $q_2 = 0.01$ m, $\beta_1 = -0.0003$, and $\beta_2 = 0.0302$ m. The use of these parameters for simulation purposes is meaningful as decaWave DW1000 UWB nodes are currently considered for experimental implementation of the proposed localization system.

We remark that the considered SS-based approach to TDoA-based localization does not depend on the specific statistical measurement error model. In other words, provided that the communication standard does not change (namely, IEEE 802.15.4a is used), the use of other UWB nodes (different from decaWave DW1000) would require to change the values of the parameters in equations (3) and (4). However, the considered method would still apply.

III. LOCALIZATION STRATEGY

A. Positioning Algorithms

TDoA-based 3D positioning *geometric* algorithms leverage the geometric structure of the scenario to determine the unknown target position. In particular, standard geometric algorithms determine the target position by solving a linear system of equations of the following type:

$$\boldsymbol{E}\boldsymbol{s} = \boldsymbol{b} \qquad (5)$$

where $\boldsymbol{E}$ and $\boldsymbol{b}$ are proper matrix and vector depending on the specific scenario, i.e., the anchors' positions and the anchor-target distance measurements. Assume (for notational simplicity) that $\boldsymbol{a}_1$ is the first anchor which receives the beacon from the target, i.e., $\tau' = \tau_1$.

The Linear Hyperbolic Positioning System (LinHPS) [28] is our geometric algorithm of choice. In this case, $\boldsymbol{E}$ is a matrix of size $\binom{N-1}{2} \times 3$ and $\boldsymbol{b}$ is a vector of size $\binom{N-1}{2}$ defined, respectively, as follows:

$$\boldsymbol{E} = \left[\boldsymbol{E}_2^T, \boldsymbol{E}_3^T, \ldots, \boldsymbol{E}_{N-1}^T\right]^T$$
$$\boldsymbol{b} = \left[\boldsymbol{b}_2^T, \boldsymbol{b}_3^T, \ldots, \boldsymbol{b}_{N-1}^T\right]^T$$

with

$$\boldsymbol{E}_i = \left[\boldsymbol{e}_{i,i+1}^T, \boldsymbol{e}_{i,i+2}^T, \ldots, \boldsymbol{e}_{i,N}^T\right]^T$$
$$\boldsymbol{b}_i = [b_{i,i+1}, b_{i,i+2}, \ldots, b_{i,N}]^T \qquad i = 2, 3, \ldots, N-1$$

where

$$\boldsymbol{e}_{ik} = 2c\left[\widetilde{\Delta\tau}_k(\boldsymbol{a}_i - \boldsymbol{a}_1) - \widetilde{\Delta\tau}_i(\boldsymbol{a}_k - \boldsymbol{a}_1)\right]$$
$$b_{ik} = c\left[\widetilde{\Delta\tau}_i\left(c^2\widetilde{\Delta\tau}_k^2 - \|\boldsymbol{a}_k\|^2\right) + \left(\widetilde{\Delta\tau}_i - \widetilde{\Delta\tau}_k\right)\|\boldsymbol{a}_1\|^2 + \widetilde{\Delta\tau}_k\left(\|\boldsymbol{a}_i\|^2 - c^2\widetilde{\Delta\tau}_i^2\right)\right].$$

The LS solution of system (5) is

$$\hat{\boldsymbol{s}} = \boldsymbol{E}^+\boldsymbol{b}$$

being $\boldsymbol{E}^+$ the Moore-Penrose pseudoinverse of $\boldsymbol{E}$ [29], as $\boldsymbol{E}$ is not, in general, a square matrix. Note that solving (5) has a complexity on the order of $O(N^2)$ [30].

The performance of LinHPS has been compared with those of other algorithms, either geometric or from the soft computing domain. In the former case, the Plane Intersection (PI) [31] and the Two-Stage Maximum-Likelihood (TSML) [32] algorithms have been considered. In the latter case, Particle Swarm Optimization (PSO) [33] has been used. Our results, not shown here for lack of space, show that the considered LinHPS-based scheme employing all the available anchors achieves the best localization accuracy. Moreover, the use of the SS strategy (introduced in the following Subsection III-B) improves the performance of the "standard" LinHPS-based scheme (i.e., using *all* the available anchors), allowing to approach the CRLB (as will be shown in Section IV). In this sense, the LinHPS-based SS strategy achieves the best performance among all considered algorithms. Finally, the inherent iterative nature of the PSO leads to a computational complexity which may be unfeasible in most realistic applications with strict latency and computational constraints (e.g., in particular IoT scenarios).

B. Subset Selection

In [23], it has been shown that the main drawback of the LinHPS with all the anchors closely placed on the hotspot is that the performance degrades in the presence of symmetries, with respect to the target position, in the anchors' placement. In fact, standard localization algorithms use all the anchors, under the assumption that they all have the same reliability

(since the noise statistical model is the same for all the anchors). However, the presence of geometric symmetries may hinder the solution of the localization problem. This is due to the fact that some anchors may be collinear with respect to a proper plane. In order to avoid this, one can heuristically move the anchors by a few centimeters (e.g., 10 cm). Our results, not shown here for conciseness, do not show any relevant improvement. This is due to the fact that, especially at large target-hotspot distances, the anchors are still almost collinear with respect to the target. This motivated us to consider SS.

Although, in principle, an optimal algorithm should rely on all available measurements, its derivation may be challenging and its complexity may be high. Rather than deriving this algorithm, in this subsection we consider a simple approach, denoted as SS, to improve the performance of a standard (i.e., link quality-agnostic) positioning algorithm. The key idea of this paper is to "strongly break" such symmetries by considering only subsets of anchors.

Assuming that all measurements are available, the SS strategy leads to performing localization with a subset of anchors $\mathcal{S} \subseteq \mathcal{A}$ of size $|\mathcal{S}| = N_{\mathrm{av}} \leq N$. The subset is selected, among all the available subsets with N_{av} anchors, in such a way that the corresponding anchors' relative positions (with respect to the target position) are as asymmetric as possible. In principle, any anchor can be selected for inclusion in the subset. However, in realistic scenarios some anchors may not receive the target beacon (because of obstructions) or the target-anchor communication link may be in Non-Line-Of-Sight (NLOS) condition (the corresponding distance measurement may be very noisy). Dynamic SS, based on link quality estimation, is the subject of current research activity.

Note that the asymmetries in the anchors' placement strongly depend on their relative positions with respect to the target. Since the target position is unknown, one has to choose the subset so that the anchors are (on average) asymmetrically placed for all possible target positions. To this end, the following data fusion strategy can be applied to further improve the positioning accuracy. For a given value of N_{av}, let us consider M (partially overlapping) subsets $\mathcal{S}_1, \mathcal{S}_2, \ldots, \mathcal{S}_M$, which are representative of asymmetric anchors' placements for different target positions (for instance, different sectors around the hotspot). At this point, denoting as $\hat{\boldsymbol{s}}_i$ the position estimate with the i-th subset, $i = 1, 2, \ldots, M$, one may fuse these estimates by computing the CoG of all of them, thus leading to the following (arithmetic) average estimate:

$$\hat{\boldsymbol{s}}_{\mathrm{df}} = \frac{1}{M} \sum_{i=1}^{M} \hat{\boldsymbol{s}}_i. \qquad (6)$$

The SSwDF strategy has some similarities to the Divide And Conqueror (DAC) approach proposed in [34]. The DAC approach is based on low-complexity Maximum Likelihood (ML) estimators in properly defined sub-problems and then merging together the obtained solutions to derive a final estimator. Such an approach was effectively applied to ML position estimation with AoA and TDoA measurements in [35]. However, while the goal of [35] is to achieve the same performance of standard ML solutions (without the introduction

TABLE I
ANCHORS' POSITIONS (IN METERS).

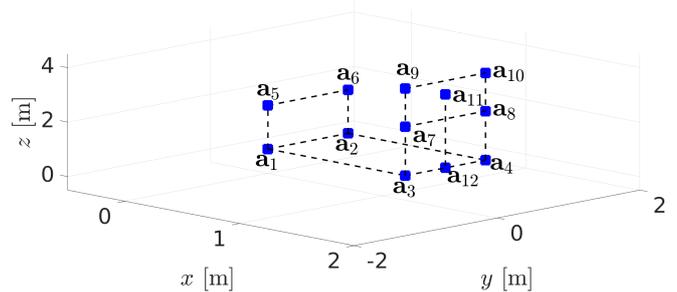| Anchor	3D coordinates [m]
$\boldsymbol{a}_1$	$[0, 0, 0.4]^T$
$\boldsymbol{a}_2$	$[0, 1.12, 0.4]^T$
$\boldsymbol{a}_3$	$[1.2, 0, 0.4]^T$
$\boldsymbol{a}_4$	$[1.2, 1.12, 0.4]^T$
$\boldsymbol{a}_5$	$[0, 0, 2]^T$
$\boldsymbol{a}_6$	$[0, 1.12, 2]^T$
$\boldsymbol{a}_7$	$[1.2, 0, 2.2]^T$
$\boldsymbol{a}_8$	$[1.2, 1.12, 2.2]^T$
$\boldsymbol{a}_9$	$[1.2, 0, 3.6]^T$
$\boldsymbol{a}_{10}$	$[1.2, 1.12, 3.6]^T$
$\boldsymbol{a}_{11}$	$[1.2, 0.56, 3.1]^T$
$\boldsymbol{a}_{12}$	$[1.2, 0.56, 0.4]^T$
$\bar{\boldsymbol{a}}$	$[0.8, 0.56, 1.725]^T$

Fig. 2. Anchors' placement for simulations.

of sub-problems) with lower complexity, in our manuscript we focus on improving the performance of the considered LinHPS positioning algorithms. In fact, the use of subsets allows to eliminate symmetries in anchors' placement, which are detrimental for the overall system performance (in terms of localization accuracy).

IV. NUMERICAL RESULTS

In order to evaluate the system performance, we consider an illustrative setup,[2] where the hotspot accommodates $N = 12$ anchors at the positions given in Table I. The approximate hotspot size is 1.5 m × 1.5 m × 4 m and the chosen placement is compliant with practical anchors' positions on an AGV.[3] A pictorial description of the considered anchors' placement is given in Fig. 2. This setup is referred to as symmetric, since there are symmetries in the anchors' placement (some of the anchors have the same value of one of the coordinates). The target coordinates are the following:

$$\boldsymbol{s} = [R\cos\theta, R\sin\theta, 1]^T$$

where R (dimension: [m]) has been defined at the end of Subsection II, whereas θ is the target angle with respect to the CoG projection on the $x - y$ plane. The target height $s_z = 1$ m is representative of a target (e.g., identification tag) worn by a person. We will consider various values for R in the range from 5 m (representative of a target close to

---

[2]Similar considerations can be carried out for any other scenario.
[3]This is relevant to allow target estimation in the surroundings of the AGV.
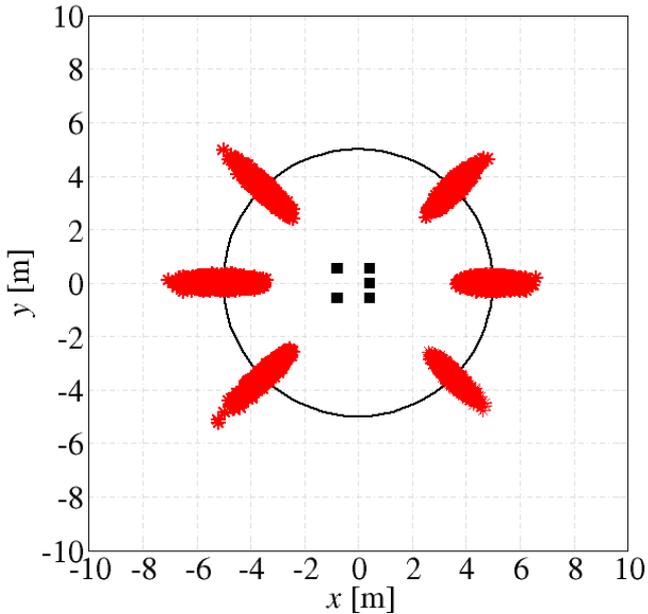
Fig. 3. Estimated positions when the target is positioned at $R = 5$ m and $\theta = 0, \pm\pi/4, \pi, \pi \pm \pi/4$.

the hotspot) to 15 m (representative of a target far from the hotspot). Moreover, $T = 10^5$ runs with independent beacon transmissions from the target are performed for statistical analysis.

We preliminarily investigate the performance of the LinHPS algorithm when all the anchors are used by the positioning algorithm. In Fig. 3, various estimated positions are shown (each point corresponds to a different simulation run) when the target is positioned at $R = 5$ m and $\theta = 0, \pm\pi/4, \pi, \pi \pm \pi/4$— at $R = 15$ m, a performance degradation is observed (the results are not shown for lack of space). It is worth noting that, for each true position, the estimates concentrate around it. Moreover, the target's AoA can be accurately estimated in all directions. As already pointed out in [36], this is due to the fact that the target AoA can be estimated by considering any pair of noisy distance estimates between the target and anchors. Moreover, the specific hotspot geometry with collinear anchors leads to very similar angle estimates for any target-anchor pair. Therefore, one can conclude that the target AoA can be accurately estimated.

We first analyze the impact of the number of anchors per subset, i.e., the parameter N_{av}. This corresponds to considering $M = 1$ (i.e., the estimate derives from a single subset). The following subsets $\mathcal{S}^{(N_{av})}$, $N_{av} \in \{6, 7, 8\}$, are considered:[4]

$$
\begin{aligned}
\mathcal{S}^{(6)} &= \{a_2, a_3, a_6, a_7, a_9, a_{11}\} \\
\mathcal{S}^{(7)} &= \{a_2, a_3, a_6, a_7, a_9, a_{11}, a_{12}\} \\
\mathcal{S}^{(8)} &= \{a_1, a_2, a_3, a_6, a_7, a_9, a_{11}, a_{12}\}.
\end{aligned}
$$

These subsets have been heuristically chosen so that the anchors' configuration is (on average) as asymmetric as possible with respect to the target position. In Fig. 4, the three-dimensional views of the chosen subsets are shown: (a) $\mathcal{S}^{(6)}$,

[4]The performance with $N_{av} \leq 5$ degrades significantly.

(b) $\mathcal{S}^{(7)}$, and (c) $\mathcal{S}^{(8)}$. In each subfigure, the anchors of the corresponding subset are highlighted in red.

We now analyze the following concise system performance indicators.

- *Localization pattern*, defined as the ensemble of average position estimates (projected on the $x - y$ plane), where the target lies along the circle with radius R.
- *Angular error*, defined as

$$\psi = \theta - \angle\hat{s} \qquad (7)$$

being $\angle\cdot$ the angle operation.
- *Distance error (with sign)*, defined as

$$d = -\text{sign}\left(|\psi| - \frac{\pi}{2}\right)(|\hat{s}| - R) \qquad (8)$$

where $\text{sign}(x)$ is the sign operation. The indicator (8) is expedient to determine if the estimated position overestimates or underestimates the true distance.

Note that (7) and (8) represent the radial and angular components of the estimation error. In fact, the results in Fig. 3 show that the AoA is well identified, whereas the estimated distance can assume values in a non-negligible range. These performance indicators may be relevant in applications where one needs to identify the region (e.g., a sector around the hotspot) where the target lies, but AoA techniques (typically based on the use of multiple antennas) are not applicable.

In Fig. 5, the localization pattern is shown considering the LinHPS algorithm with a single ($M = 1$) subset. Various values of the number N_{av} of available anchors in the subset, namely, 6, 7, 8, and 12 (if $N_{av} = 12$, all anchors are used together), are considered. One can observe that the use of SS improves the performance, i.e., the average location estimate with a smaller number of anchors (without modifying the localization algorithm) is closer to the true position than in the case with the use of all the anchors. This is due to the fact that in the considered subsets the anchors are placed, with respect to the target, asymmetrically. Moreover, it seems that $N_{av} = 6$ is the best choice, since it guarantees the best average position estimate.

In Table II, the mean and standard deviation of the distance error with sign (μ_d and σ_d, respectively) and of the angular error (μ_ψ and σ_ψ, respectively) are shown for SS and various values of N_{av} and R. For each case, the average, minimum, and maximum values, for all considered values of angle θ, are shown. It is worth noting that the conclusions drawn from Fig. 5 are confirmed in this case as well—we remark only that the standard deviations of both radial and angular errors with $N_{av} = 6$ are larger than those with $N_{av} = 7$. We can then conclude that setting $N_{av} = 7$ leads to the best tradeoff between average positioning accuracy and dispersion of the estimates around this average value. Therefore, in the remainder of this section, we will focus on a scenario with $N_{av} = 7$, considering various subsets and data fusion according to (6).
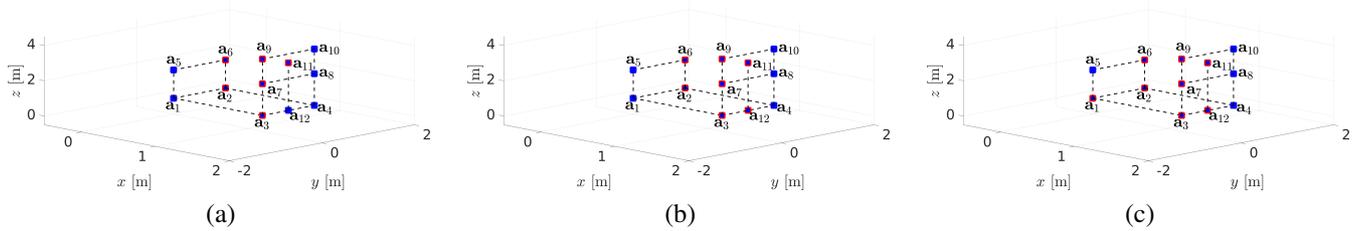
Fig. 4. Three-dimensional views of the chosen subsets: (a) $\mathcal{S}^{(6)}$, (b) $\mathcal{S}^{(7)}$, and (c) $\mathcal{S}^{(8)}$. Anchors in the subsets are highlighted in red.
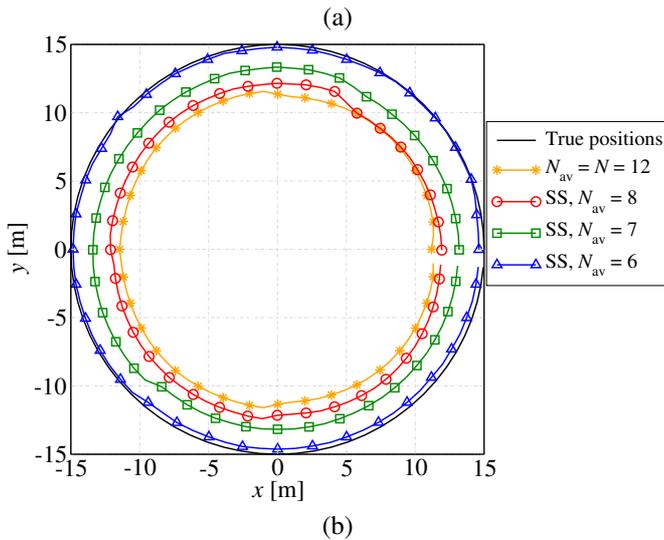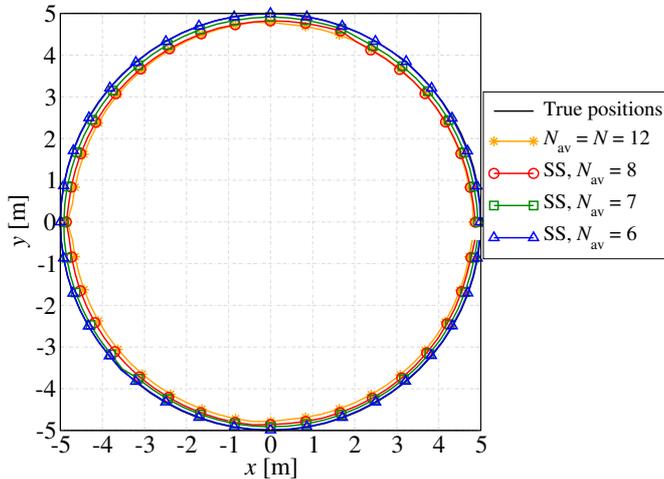

(a)

(b)

Fig. 5. Localization pattern considering the LinHPS algorithm with a single ($M = 1$) subset. Various values of the number N_{av} of available anchors in the subset, namely, 6, 7, 8, and 12, are considered.

In the SSwDF case, the following $M = 5$ selected subsets, heuristically chosen among all the possible subsets to be as much asymmetric as possible, are considered:[5]

$$\mathcal{S}_1 = \{\boldsymbol{a}_2, \boldsymbol{a}_3, \boldsymbol{a}_6, \boldsymbol{a}_7, \boldsymbol{a}_9, \boldsymbol{a}_{11}, \boldsymbol{a}_{12}\}$$
$$\mathcal{S}_2 = \{\boldsymbol{a}_1, \boldsymbol{a}_4, \boldsymbol{a}_5, \boldsymbol{a}_8, \boldsymbol{a}_{10}, \boldsymbol{a}_{11}, \boldsymbol{a}_{12}\}$$

[5]An exhaustive search among all the possible subsets has been performed and those with best localization performance have been chosen. The investigation of (possibly) optimal anchors' placement and dynamic SS may be subject of future work.

TABLE II
MEAN AND STANDARD DEVIATION OF THE DISTANCE ERROR WITH SIGN AND OF THE ANGULAR ERROR FOR SS AND VARIOUS VALUES OF N_{av} AND R. FOR EACH CASE, THE AVERAGE, MINIMUM, AND MAXIMUM VALUES, FOR ALL CONSIDERED VALUES OF ANGLE θ, ARE SHOWN.

		$R = 5$ m				$R = 15$ m			
N_{av}		12	8	7	6	12	8	7	6
μ_d [m]	AVG	-0.23	-0.17	-0.08	0	-3.53	-2.91	-1.75	-0.21
	MIN	-0.28	-0.23	-0.12	-0.02	-3.81	-3.48	-2.09	-0.42
	MAX	-0.16	-0.12	-0.01	0.02	-3.36	-2.55	-1.42	0.17
σ_d [m]	AVG	0.41	0.61	0.67	0.72	2.11	3.59	4.53	8.41
	MIN	0.37	0.46	0.5	0.52	2.02	3.18	3.92	5.22
	MAX	0.49	0.72	0.78	0.84	2.42	4.08	5.39	93.6
μ_ψ [deg]	AVG	0	0.01	0	0.04	0	0	0	0.02
	MIN	-0.15	-0.23	-0.21	-0.22	-0.33	-0.52	-0.51	-0.42
	MAX	0.15	0.27	0.2	0.29	0.33	0.67	0.48	0.46
σ_ψ [deg]	AVG	0.97	1.46	2.54	3.55	0.8	3.82	4.68	5.17
	MIN	0.93	0.95	1	1.08	0.81	2.08	2.88	3.08
	MAX	1.12	1.91	3.87	5.62	1.4	6.07	6.76	7.32

$$\mathcal{S}_3 = \{\boldsymbol{a}_1, \boldsymbol{a}_2, \boldsymbol{a}_3, \boldsymbol{a}_4, \boldsymbol{a}_5, \boldsymbol{a}_8, \boldsymbol{a}_{10}\}$$
$$\mathcal{S}_4 = \{\boldsymbol{a}_2, \boldsymbol{a}_3, \boldsymbol{a}_5, \boldsymbol{a}_6, \boldsymbol{a}_7, \boldsymbol{a}_8, \boldsymbol{a}_9\}$$
$$\mathcal{S}_5 = \{\boldsymbol{a}_1, \boldsymbol{a}_2, \boldsymbol{a}_7, \boldsymbol{a}_8, \boldsymbol{a}_9, \boldsymbol{a}_{11}, \boldsymbol{a}_{12}\}.$$

In Fig. 6, the three-dimensional views of the chosen subsets are shown: (a) $\mathcal{S}_1$, (b) $\mathcal{S}_2$, (c) $\mathcal{S}_3$, (d) $\mathcal{S}_4$, and (e) $\mathcal{S}_5$. In each subfigure, the anchors of the corresponding subset are highlighted in red. It can be observed that, even though some symmetries may still exist (depending on the relative target-hotspot position), most of these symmetries disappear.

During our tests, we observed that estimates' outliers may appear, i.e., one (or more) of the position estimates, associated with some of the considered subsets, can significantly differ from the others, thus biasing the average in (6) in the SSwDF case. This limitation can be overcome by eliminating outliers before averaging—this outlier elimination is practically feasible by checking if its distance from the others is over a pre-defined threshold.

In Fig. 7, the position estimates are shown when the target is positioned at $\theta = 0, \pm\pi/4, \pi, \pi \pm \pi/4$, for $R = 5$ m and $N_{\mathrm{av}} = 7$, comparing (a) SS with $M = 1$ (no data fusion) and (b) SSwDF with $M = 5$. Comparing the results in Fig. 7 with those in Fig. 3, one can observe that, although the use of a single subset improves the average localization performance, the dispersion of the estimates increases (as also observed in Table II). On the other hand, the SSwDF approach with $M = 5$ drastically improves the positioning accuracy, since the position estimates concentrate around the true value.

In Fig. 8, the distance error with sign is shown, as a function of R, for $\theta = 0°$—similar considerations hold for other values of θ—and various subsets comparing the performance without data fusion (i.e., single subset) and with data fusion (SSwDF with $M = 5$). The confidence interval $\mu \pm \sigma$ is also shown. In
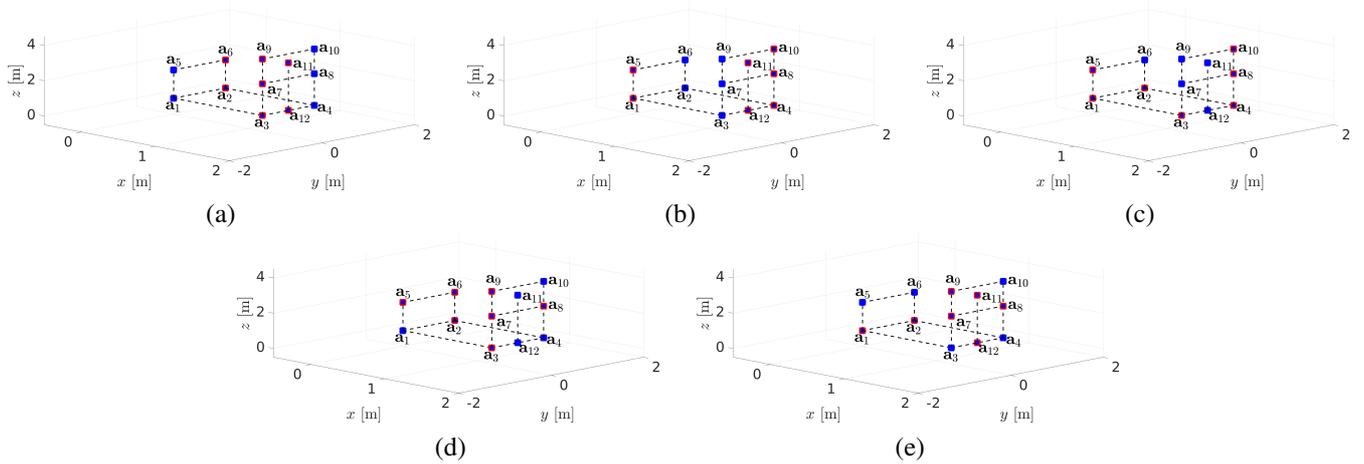
Fig. 6. Three-dimensional views of the chosen subsets: (a) $\mathcal{S}_1$, (b) $\mathcal{S}_2$, (c) $\mathcal{S}_3$, (d) $\mathcal{S}_4$, and (e) $\mathcal{S}_5$. Anchors in the subsets are highlighted in red.

case (a), the absolute value is shown, whereas in case (b) the relative value, with respect to R is considered. The average distance error is approximately the same for all the subsets, but the standard deviation can be drastically reduced using data fusion. As expected, increasing the distance leads to a minor performance degradation in terms of average error (from a few centimeters to at most 2 m), but the standard deviation increases. This corresponds to an increase of approximately 1% (for $R = 5$ m) to 10% (for $R = 15$ m). This is due to the noise model in (3)-(4), in which the standard deviation of the measured ToF increases with the target-anchor distance, thus leading to a worse localization accuracy for increasing values of the hotspot-target distance R.

In Fig. 9, the angular error is shown, as a function of R, for $\theta = 0°$ and various subsets (comparing the performance without and with data fusion). The confidence interval $\mu \pm \sigma$ is also shown—similar considerations hold for other values of θ. Considerations similar to those carried out for the distance error with sign in Fig. 8 apply here. However, it is worth noting that the standard deviation has a bimodal behaviour, namely: below a given threshold distance (between 10 m and 12 m), it is approximately constant, whereas above this threshold it rapidly increases. Moreover, it can also be observed that the use of data fusion does not always lead to a standard deviation reduction at longer distances. As an example, at $R = 15$ m the use of $\mathcal{S}_2$ leads to a small standard deviation, but the use of $\mathcal{S}_4$ leads to larger standard deviation. In this case, data fusion worsens the overall performance with respect to that of $\mathcal{S}_2$. An interesting research direction is the derivation of adaptive data fusion strategies with dynamic SS.

In Table III, the mean and standard deviation of the distance error with sign and of the angular error are summarized for scenarios without SS ($N_{\mathrm{av}} = 12$) and with SSwDF ($N_{\mathrm{av}} = 7$ with $M = 5$), considering two values of R. For each case, the average, minimum, and maximum values for all considered values of the angle θ are shown. The relative percentage, with respect to the true distance R, is shown between round brackets for the distance error with sign. One can observe that, for both values of R, the distance error with sign drastically reduces towards zero, i.e., the target-hotspot

TABLE III
MEAN AND STANDARD DEVIATION OF THE DISTANCE ERROR WITH SIGN AND OF THE ANGULAR ERROR FOR SCENARIOS WITHOUT SS ($N_{\mathrm{av}} = 12$) AND WITH SSWDF ($N_{\mathrm{av}} = 7$ WITH $M = 5$), CONSIDERING TWO VALUES OF R. FOR EACH CASE, THE AVERAGE, MINIMUM, AND MAXIMUM VALUES FOR ALL CONSIDERED VALUES OF THE ANGLE θ ARE SHOWN.

| | | $R = 5$ m | | $R = 15$ m | |
		w/o SS	SSwDF	w/o SS	SSwDF
μ_d [m]	AVG	-0.23 (-4.6%)	-0.08 (-1.6%)	-3.53 (-23.5%)	-1.62 (-1.62%)
	MIN	-0.28 (-5.6%)	-0.11 (-2.2%)	-3.81 (-25.4%)	-1.93 (-12.9%)
	MAX	-0.16 (-3.2%)	-0.06 (-1.2%)	-3.36 (-22.4%)	-1.44 (-9.6%)
σ_d [m]	AVG	0.41 (8.2%)	0.29 (5.8%)	2.11 (14.1%)	2.02 (13.5%)
	MIN	0.37 (7.4%)	0.26 (5.2%)	2.02 (13.5%)	1.87 (12.5%)
	MAX	0.49 (9.8%)	0.34 (6.8%)	2.42 (16.1%)	2.22 (14.8%)
μ_ψ [deg]	AVG	0	-0.01	0	-0.01
	MIN	-0.15	-0.08	-0.33	-0.2
	MAX	0.15	0.05	0.33	0.12
σ_ψ [deg]	AVG	0.97	0.91	0.8	2.21
	MIN	0.93	0.85	0.81	1.13
	MAX	1.12	0.98	1.4	3.01

distance is well measured. On the other hand, the angular error slightly increases. However, it remains limited and, therefore, it can be concluded that the target AoA is still well estimated in all cases.

We finally analyze the localization error in terms of the estimated Root Mean Square Error (RMSE), defined as follows:

$$\mathrm{RMSE} \triangleq \frac{1}{T} \sum_{i=1}^{T} ||\boldsymbol{s} - \hat{\boldsymbol{s}}^{(k)}||$$

where $\hat{\boldsymbol{s}}^{(k)}$ denotes the estimated (3D) position at the k-th simulation run ($k = 1, 2, \ldots, T$). The RMSE can be compared with a theoretical benchmark given by the CRLB on the positioning error. In particular, we resort to the approach proposed in [37] for the calculation of the CRLB, based on the assumption of zero-mean and constant (with respect to the target-anchor distance) variance TDoA measurements. Even if
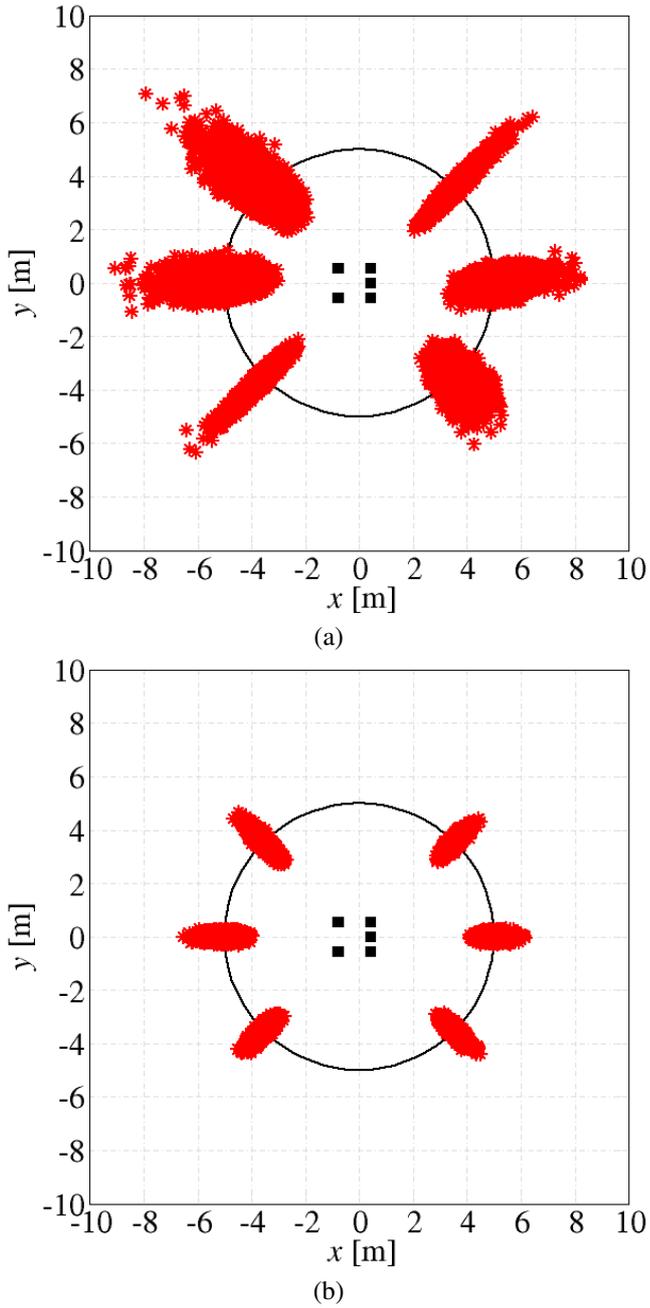
Fig. 7. Position estimates when the target is positioned at $\theta = 0, \pm\pi/4, \pi, \pi \pm \pi/4$, for $R = 5$ m and $N_{\text{av}} = 7$, comparing (a) SS with $M = 1$ (no data fusion) and (b) SSwDF with $M = 5$.

our noise measurement model (3)-(4) assumes a measurement noise with non-zero mean and variance linearly dependent on the target-anchor distance, the approach in [37] allows to derive a reasonable performance benchmark, provided that the correct noise variance is considered for each target-anchor distance.[6] In particular, following the derivation in [37] one can write:

$$\text{CRLB} = \sqrt{\text{tr}\left\{\boldsymbol{J}^{-1}(\boldsymbol{s}, \{\boldsymbol{a}_i\}_{i=1}^N)\right\}}$$

[6]Note that the CRLB for UWB TDoA-based positioning is also derived in [38], [39] for another noise model, which assumes an exponential dependence of the variance with respect to the target-anchor distance. This, however, is not coherent with our model.
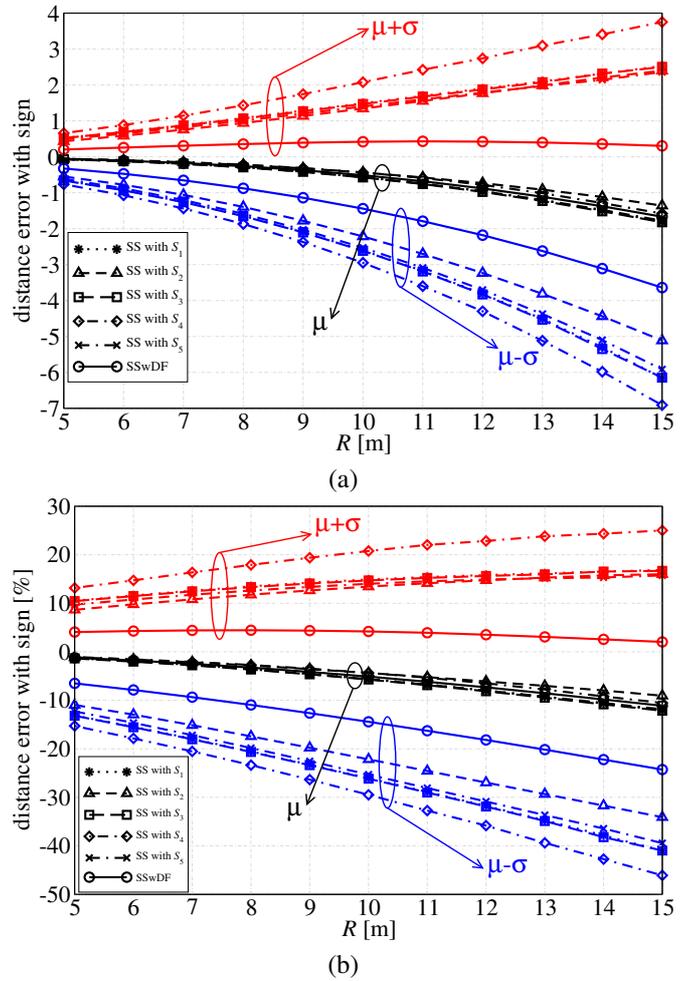

Fig. 8. Distance error with sign, as a function of R, for $\theta = 0°$ and various subsets (comparing the performance without and with data fusion). The confidence interval $\mu \pm \sigma$ is also shown. In case (a), the absolute value is shown, whereas in case (b) the relative value, with respect to R, is considered.
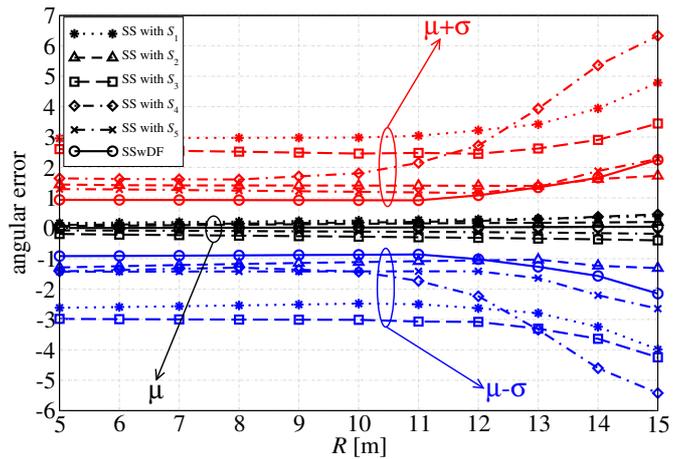

Fig. 9. Angular error, as a function of R, for $\theta = 0°$ and various subsets (comparing the performance without and with data fusion). The confidence interval $\mu \pm \sigma$ is also shown.
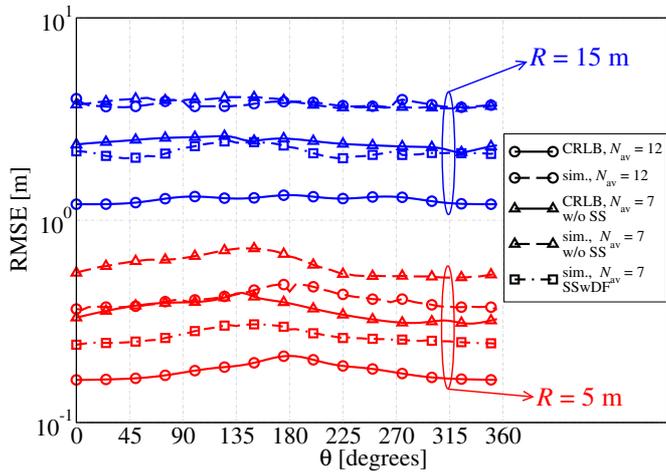
Fig. 10. Positioning error, as a function of the target-hotspot angle, for various values of the target-hotspot distance R. The performance of various positioning schemes is compared with the theoretical CRLB.

where: $\mathrm{tr}\{\cdot\}$ is the trace operator; $\boldsymbol{J}$ is the so-called Fisher information matrix (in the current case, it is 3×3 matrix); and $\boldsymbol{J}^{-1}$ is the inverse of $\boldsymbol{J}$. The generic element of the Fisher information matrix can be written as

$$J_{k\ell} = \frac{1}{\sigma^2_{\mathrm{CRLB}}} \sum_{i=1}^{N-1} \sum_{j=i}^{N} \left[\frac{s_k - a_k^{(i)}}{r_i} - \frac{s_k - a_k^{(j)}}{r_j} \right]$$
$$\times \left[\frac{s_\ell - a_\ell^{(i)}}{r_i} - \frac{s_\ell - a_\ell^{(j)}}{r_j} \right] \quad k,\ell \in \{x,y,z\}$$

where σ_{CRLB} is the standard deviation of the noisy measurements of the range difference, which is assumed to be constant. The standard deviation in (4) is associated with a ToA approach and depends on the anchor-target distance. Since a range difference measurement corresponds to the difference between two Gaussian-distributed range measurements (with the same standard deviation), the range difference measurement has a Gaussian distribution with standard deviation equal to $\sqrt{2}$ times the one of the range measurements. Considering the standard deviation in correspondence to the arithmetic average of the distances between the target and all anchors, from (4) we define:

$$\sigma_{\mathrm{CRLB}} \triangleq \sqrt{2} \left[\beta_1 \left(\frac{1}{N} \sum_{i=1}^{N} r_i \right) + \beta_2 \right].$$

In Fig. 10, the positioning error is shown, as a function of the target-hotspot angle, for various values of the target-hotspot distance R. The performance of various positioning schemes (without and with data fusion) is compared with the theoretical CRLB. As already observed before, moving from $N_{\mathrm{av}} = 12$ (namely, using all the anchors) to $N_{\mathrm{av}} = 7$ with a single subset, the performance degrades due to the fact that the variances of both angle and distance estimates increase. However, using 5 subsets with data fusion allows to improve the performance, moving closer to the theoretical benchmark given by the CRLB with $N_{\mathrm{av}} = 12$. We remark that the comparison with the CRLB with $N_{\mathrm{av}} = 12$ is meaningful,

TABLE IV
AVERAGE (OVER THE TARGET-HOTSPOT ANGLE) ESTIMATION ERROR (IN METERS) FOR THE SCHEMES CONSIDERED IN FIG. 10.

Scheme	$R = 5$ m	$R = 15$ m
Benchmark (CRLB with $N_{\mathrm{av}} = 12$)	0.18	1.27
LinHPS (with $N_{\mathrm{av}} = 12$)	0.41	3.73
w/o SS (with $N_{\mathrm{av}} = 7$)	0.6	3.79
SSwDF (with $N_{\mathrm{av}} = 7$)	0.27	2.19

as the scheme with data fusion encompasses all anchors (i.e., the union of the considered subsets includes all anchors).

In Table IV, we summarize the average (over the target-hotspot angle) estimation error (in meters) for the schemes considered in Fig. 10. It is worth noting that SSwDF allows to reduce the average estimation error of approximately 35% with respect to the LinHPS using all the anchors. Moreover, the final performance is relatively close to the theoretical benchmark limit predicted by the CRLB.

V. IMPACT OF SYNCHRONIZATION ERROR

While in the previous section we have analyzed the system performance under the assumption of perfect time synchronization among the anchors, we now investigate the impact of imperfect synchronization. In fact, the reliability of a TDoA localization algorithm strictly depends on clock synchronization between the anchors. As already outlined in [40], a synchronization bias ϵ_i affecting the ToF measurements consists of a shift of the mean value of the ToF measurement μ_i introduced in Subsection II-B, i.e.,

$$\mu_i = \overline{\nu}_i / c + \epsilon_i. \quad (9)$$

The inter-anchor synchronization bias ϵ_i is modeled as a random variable with mean η_{sync}, uniformly distributed in the interval $[\eta_{\mathrm{sync}}(1 - \alpha_{\mathrm{sync}}), \eta_{\mathrm{sync}}(1 + \alpha_{\mathrm{sync}})]$, where η_{sync} and α_{sync} are proper parameters to be experimentally set. This model is representative of a random clock drift around a deterministic (known) parameter η_{sync}.

In Fig. 11, the RMSE is shown for various synchronization levels (i.e., values of η_{sync} and α_{sync}) and target-hotspot distances (namely, $R = 5$ m and $R = 15$ m), comparing the performance without SS and with SSwDF. The simulation setup is the same of Section IV. The target-hotspot angle θ is set to $0°$—similar considerations hold for other angles. It can be observed that the presence of a synchronization bias leads to a clear performance degradation; in particular, the stronger the synchronization bias, the more significant such a degradation. One can see that the RMSE increase starts to be significant, for every value of α_{sync} and R, for $\eta_{\mathrm{sync}} > 1$ ns. This can be considered as a guideline for hardware design in order to achieve good performance with the proposed TDoA-based scheme. Moreover, the use of SS leads to a performance improvement. This means that in the presence of SS and data fusion the synchronization bias becomes less crucial; however, it is still true that $\eta_{\mathrm{sync}} = 1$ ns is a critical value to obtain a limited performance degradation. Such limit can be practically achieved with cabled anchors, by developing an accurate clock source distribution able to guarantee a precise timing synchronization between devices [41].
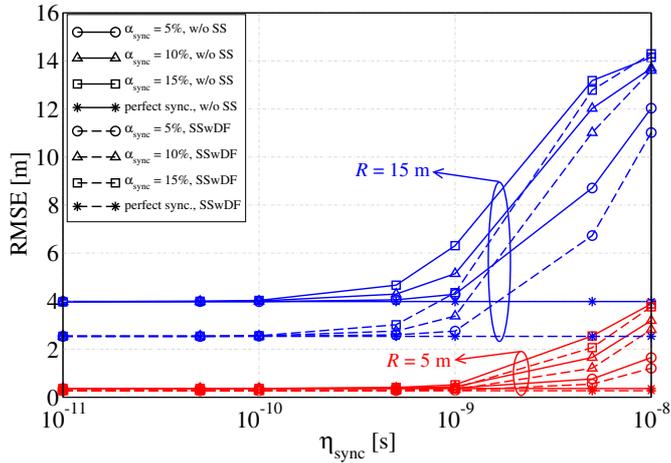
Fig. 11. RMSE for various synchronization levels and target-hotspot distances, comparing the performance without SS and with SSwDF.

VI. Concluding Remarks

In this paper, we have tackled the problem of determining a target position using UWB communications and TDoA-based processing at the anchors. We have considered a scenario with anchors placed on a single hotspot (with sufficiently small dimensions) and the target moving around it. Since our results show that the localization accuracy reduces if the anchors exhibit symmetries in their placement, we have considered a SS method to break such symmetries. Our results show that, with a geometric algorithm (LinHPS), the target AoA can be estimated with an average error of at most $3°$ when the target is at 15 m, while the distance is typically underestimated (average errors of at most 10 cm and 4 m can be obtained at distance R equal to 5 m and 15 m, respectively). The use of data fusion allows to further improve the performance, allowing to approach the theoretical performance limit predicted by the CRLB. Finally, the impact of a synchronization error between anchors, modeled as a bias, has been investigated, showing that a bias on the order of 1 ns leads to a significant localization accuracy degradation. Future work will be devoted to the design of dynamic SS strategies to take into account NLOS conditions due to the specific environment and hotspot design.

References

[1] J. A. Del Peral-Rosado, R. Raulefs, J. A. López-Salcedo, and G. Seco-Granados, "Survey of cellular mobile radio localization methods: From 1G to 5G," *IEEE Commun. Surveys Tutorials*, vol. 20, no. 2, pp. 1124–1148, 2018, DOI: 10.1109/COMST.2017.2785181.

[2] L. Atzori, A. Iera, and G. Morabito, "The Internet of Things: A survey," *Elsevier Computer Networks*, vol. 54, no. 15, pp. 2787–2805, October 2010, DOI: 10.1016/j.comnet.2010.05.010.

[3] D. Irwin and J. Albrecht, "Smart homes: Implemented," *IEEE Pervasive Computing*, vol. 18, no. 2, pp. 91–95, April 2019, DOI: 10.1109/MPRV.2019.2912258.

[4] J. Zhang, "Bridging the physical, the digital, and the social," *IEEE Internet of Things Magazine*, vol. 2, no. 1, pp. 8–9, March 2019, DOI: 10.1109/MIOT.2019.8835418.

[5] P. P. Gaikwad, J. P. Gabhane, and S. S. Golait, "A survey based on smart homes system using Internet-of-Things," in *Int. Conf. Computation of Power, Energy, Information and Communication* (ICCPEIC), April 2015, pp. 0330–0335, DOI: 10.1109/ICCPEIC.2015.7259486.

[6] P. Patel, M. I. Ali, and A. Sheth, "From raw data to smart manufacturing: AI and semantic Web of Things for Industry 4.0," *IEEE Intelligent Systems*, vol. 33, no. 4, pp. 79–86, July 2018, DOI: 10.1109/MIS.2018.043741325.

[7] T.-H. Chiang, Z.-H. Sun, H.-R. Shiu, . C.-J. Lin, and Y.-C. Tseng, "Magnetic field-based localization in factories using neural network with robotic sampling," *IEEE Sensors J.*, vol. 20, no. 21, pp. 13 110–13 118, November 2020, DOI: 10.1109/JSEN.2020.3003404.

[8] F. Shamsfakhr, L. Palopoli, D. Fontanelli, A. Motroni, and A. Buffi, "Robot localisation using UHF-RFID tags for industrial IoT applications," in *IEEE Int. Workshop on Metrology for Industry 4.0 & IoT*, Rome, Italy (held as virtual), June 2020, pp. 659–664, DOI: 10.1109/MetroInd4.0IoT48571.2020.9138210.

[9] L. Barbieri, M. Brambilla, A. Trabattoni, S. Mervic, and M. Nicoli, "UWB localization in a smart factory: Augmentation methods and experimental assessment," *IEEE Trans. Instrumentation and Measurement*, vol. 70, pp. 1–18, 2021, DOI: 10.1109/TIM.2021.3074403.

[10] L. Cavanini, P. Cicconi, A. Freddi, M. Germani, S. Longhi, A. Monteriu, E. Pallotta, and M. Prist, "A preliminary study of a cyber physical system for Industry 4.0: Modelling and co-simulation of an AGV for smart factories," in *IEEE Int. Workshop on Metrology for Industry 4.0 & IoT*, Brescia, Italy, April 2018, pp. 169–174, DOI: 10.1109/METROI4.2018.8428334.

[11] L. Mo and C. Li, "Passive UHF-RFID localization based on the similarity measurement of virtual reference tags," *IEEE Trans. Instrumentation and Measurement*, vol. 68, no. 8, pp. 2926–2933, August 2019, DOI: 10.1109/TIM.2018.2869408.

[12] R. M. Buehrer, H. Wymeersch, and R. M. Vaghefi, "Collaborative sensor network localization: Algorithms and practical issues," *Proc. IEEE*, vol. 106, no. 6, pp. 1089–1114, June 2018, DOI: 10.1109/JPROC.2018.2829439.

[13] F. Zafari, A. Gkelias, and K. Leung, "A survey of indoor localization systems and technologies," *IEEE Commun. Surveys Tutorials*, vol. 21, no. 3, pp. 2568–2599, 2019, DOI: 10.1109/COMST.2019.2911558.

[14] Z. Sahinoglu, S. Gezici, and I. Guvenc, *Ultra-wideband positioning systems*. New York, NY, USA: Cambridge University Press, 2008.

[15] S. Gezici and H. V. Poor, "Position estimation via ultra-wide-band signals," *Proc. IEEE*, vol. 97, no. 2, pp. 386–403, February 2009, DOI: 10.1109/JPROC.2008.2008840.

[16] H. Liu, H. Darabi, P. Banerjee, and J. Liu, "Survey of wireless indoor positioning techniques and systems," *IEEE Trans. Systems, Man, and Cybernetics, Part C (Applications and Reviews)*, vol. 37, no. 6, pp. 1067–1080, November 2007, DOI: 10.1109/TSMCC.2007.905750.

[17] R. Zandian and U. Witkowski, "Implementation challenges of synchronisation of UWB nodes in TDoA structures," in *Int. Conf. Indoor Positioning and Indoor Navigation* (IPIN), Nantes, France, September 2018, pp. 1–8, DOI: 10.1109/IPIN.2018.8533796.

[18] H. J. Kim, Y. Xie, H. Yang, C. Lee, and T. L. Song, "An efficient indoor target tracking algorithm using TDOA measurements with applications to ultra-wideband systems," *IEEE Access*, vol. 7, pp. 91 435–91 445, 2019, DOI: 10.1109/ACCESS.2019.2927005.

[19] S. He and X. Dong, "High-accuracy localization platform using asynchronous time difference of arrival technology," *IEEE Trans. Instrumentation and Measurement*, vol. 66, no. 7, pp. 1728–1742, July 2017, DOI: 10.1109/TIM.2017.2666278.

[20] Q. Liang, B. Zhang, C. Zhao, and Y. Pi, "TDoA for passive localization: Underwater versus terrestrial environment," *IEEE Trans. Parallel and Distributed Syst.*, vol. 24, no. 10, pp. 2100–2108, October 2013, DOI: 10.1109/TPDS.2012.310.

[21] Y. Liu, L. Yang, and J. Li, "Robust UWB indoor position tracking using TDOA measurements," in *IEEE Int. Conf. Computer and Commun.* (ICCC), Beijing, China, August 2018, pp. 736–743, DOI: 10.1109/CompComm.2018.8780881.

[22] L. Huang and C. C. Ko, "Performance of maximum-likelihood channel estimator for UWB communications," *IEEE Commun. Lett.*, vol. 8, no. 6, pp. 356–358, June 2004, DOI: 10.1109/LCOMM.2004.831330.

[23] M. Martalò, G. Ferrari, S. Perri, G. Verdano, F. D. Mola, and F. Monica, "UWB TDoA-based positioning using a single hotspot with multiple anchors," in *IEEE Int. Conf. Computing, Communication and Security* (ICCCS), Rome, Italy, October 2019.

[24] S. Li and K. C. Ho, "Accurate and effective localization of an object in large equal radius scenario," *IEEE Trans. Wireless Commun.*, vol. 15, no. 12, pp. 8273–8285, December 2016, DOI: 10.1109/TWC.2016.2613534.

[25] A. Alarifi, A. Al-Salman, M. Alsaleh, A. Alnafessah, S. Al-Hadhrami, M. A. Al-Ammar, and H. S. Al-Khalifa, "Ultra wideband indoor

positioning technologies: Analysis and recent advances," *MDPI Sensors*, vol. 16, no. 5, pp. 1–36, 2016, DOI: 10.3390/s16050707.

[26] S. Monica and G. Ferrari, "An experimental model for UWB distance measurements and its application to localization problems," in *Int. Conf. Ultra-WideBand* (ICUWB), Paris, France, September 2014, pp. 297–302, DOI: 10.1109/ICUWB.2014.6958996.

[27] "decaWave DW1000," URL: `http://www.decawave.com/products/dwm1000-module`.

[28] R. Bucher and D. Misra, "A synthesizable VHDL model of the exact solution for three-dimensional hyperbolic positioning system," *VLSI Design*, vol. 15, no. 2, pp. 507–520, 2002, DOI: 10.1080/1065514021000012129.

[29] Å. Björck, *Linear Algebra and its Applications*. Elsevier Science Publishers, 1987.

[30] H. Cui, Y. Liang, C. Zhou, and N. Cao, "Localization of large-scale wireless sensor networks using Niching particle swarm optimization and reliable anchor selection," *Hindawi Wireless Commun. Mobile Comput.*, December 2018, article ID 2473875, DOI: 10.1155/2018/2473875.

[31] R. O. Schmidt, "A new approach to geometry of range difference location," *IEEE Trans. Aerosp. Electron. Syst.*, vol. AES-8, no. 6, pp. 821–835, November 1972, DOI: 10.1109/TAES.1972.309614.

[32] K. C. Ho and W. Xu, "An accurate algebraic solution for moving source location using TDOA and FDOA measurements," *IEEE Trans. Signal Processing*, vol. 52, no. 9, pp. 2453–2463, September 2004, DOI: 10.1109/TSP.2004.831921.

[33] S. Monica and G. Ferrari, "Swarm intelligent approaches to auto-localization of nodes in static UWB networks," *Applied Soft Computing*, vol. 25, pp. 426–434, December 2014, DOI: 10.1016/j.asoc.2014.07.025.

[34] J. S. Abel, "A divide and conquer approach to least-squares estimation," *IEEE Trans. Aerosp. Electron. Syst.*, vol. 26, no. 2, pp. 423–427, March 1990, DOI: 10.1109/7.53453.

[35] A. Urruela, A. Pages-Zamora, and J. Riba, "Divide-and-conquer based closed-form position estimation for AOA and TDOA measurements," in *Proc. IEEE Intern. Conf. on Acoustics, Speech, and Signal Proc.* (ICASSP), vol. 4, Toulouse, France, May 2006, DOI: 10.1109/ICASSP.2006.1661120.

[36] S. Tomic, M. Beko, R. Dinis, and P. Montezuma, "Estimating directional data from network topology for improving tracking performance," *MDPI Journal of Sensor and Actuator Networks*, vol. 8, no. 2, 2019, DOI: 10.3390/jsan8020030.

[37] L. Zwirello, T. Schipper, M. Jalilvand, and T. Zwick, "Realization limits of impulse-based localization system for large-scale indoor applications," *IEEE Trans. Instrumentation and Measurement*, vol. 64, no. 1, pp. 39–51, January 2015, DOI: 10.1109/TIM.2014.2332241.

[38] J. Xu, M. Ma, and C. L. Law, "Theoretical lower bound for UWB TDOA positioning," in *Proc. IEEE Global Telecommun. Conf.* (GLOBECOM), Washington, DC, USA, December 2007, pp. 4101–4105, DOI: 10.1109/GLOCOM.2007.780.

[39] D. B. Jourda, D. D. Dardari, and M. Z. Win, "Position error bound for UWB localization in dense cluttered environments," *IEEE Trans. Aerosp. Electron. Syst.*, vol. 44, no. 2, pp. 613–628, April 2008, DOI: 10.1109/TAES.2008.4560210.

[40] S. Busanelli and G. Ferrari, "Improved ultra wideband-based tracking of twin-receiver automated guided vehicles," *Integrated Computer-Aided Engineering*, vol. 19, no. 1, pp. 3–22, 2012, DOI: 10.3233/ICA-2012-0390.

[41] S. Leugner, M. Pelka, and H. Hellbrück, "Comparison of wired and wireless synchronization with clock drift compensation suited for U-TDoA localization," in *Workshop on Positioning, Navigation and Communication* (WPNC), Bremen, Germany, 2016, pp. 1–4, DOI: 10.1109/WPNC.2016.7822846.

Simone Perri received his degree in Mathematics from University of Parma in 2014. He worked from 2014 to 2016 as research fellow at the University of Parma. Since May 2016 he's working in E80 Research & Development team.

Gianmichele Verdano graduated in Computer Engineering at the University of Parma in 2010. He worked as R&D Engineer for a motorsport company from 2011 to 2016. Since February 2016, he has been working for Elettric80 as R&D Engineer, and since 2020 as R&D Project Leader.

Francesco De Mola received his degree in Computer Engineering from University of Modena and Reggio Emilia in 2005 and his Ph.D degree in ICT - Computer Engineering and Science from the same University in 2008. Since 2008, he's working in E80 Research & Development team, and since 2014 he holds the role of R&D Team Leader.

Francesco Monica graduated in Computer Engineering at the University of Parma in 2003 and received his Ph.D. degree in ICT in 2006. He worked as R&D Team Leader for a provider of CCTV systems from 2006 to 2015, leading the Computer Vision R&D group of the company. Since July 2015, he has been working for Elettric80 as R&D Project Manager.

Marco Martalò (SM'16) received the Ph.D. in Information Technologies from the University of Parma, Italy, in 2009. From 2012 to 2017, he was an Assistant Professor with E-Campus University, Italy, and also a Research Associate with the University of Parma, Italy, until 2020. Since 2020, he is an Associate Professor of Telecommunications at the University of Cagliari, Italy, where he is part of the Networks for Humans (Net4U) laboratory. He has co-authored the book "Sensor Networks with IEEE 802.15.4 Systems: Distributed Processing, MAC, and Connectivity. His research interests are in the design of communication, and signal processing algorithms for wireless systems and networks.

Gianluigi Ferrari is an Associate Professor of telecommunications at the University of Parma, Italy, where he received his PhD in Information Technologies in 2002. Since September 2006 he has been the Coordinator of the Internet of Things (IoT) Laboratory (http://iotlab.unipr.it/) and, since 2016, he has been the co-founder and President of things2i s.r.l. (http://www.things2i.com/), a spin-off company of the University of Parma dedicated to IoT and smart systems. His research activities revolve around signal processing, communication/networking, and IoT. He has published and consulted extensively in these areas, coordinating several technical projects, including EU-funded competitive projects. He is currently the Head of the Bachelors Degree in Computer Engineering, Electronics and Telecommunications of the University of Parma (https://cdl-iiet.unipr.it/) and a member of the Scientific Council of the Advanced Research & Technology for EMbedded Intelligent Systems (ARTEMIS) association. He is an IEEE Senior Member.